Seismic Behavior and Design of Unbonded Post-Tensioned Precast Concrete Frames

Magdy T. El-Sheikh, Ph.D.
Lecturer
Department of Structural Engineering
Cairo University
Cairo, Egypt

Richard Sause, Ph.D., P.E.
Associate Professor
Department of Civil and Environmental Engineering
Lehigh University
Bethlehem, Pennsylvania

Stephen Pessiki, Ph.D.
Associate Professor
Department of Civil and Environmental Engineering
Lehigh University
Bethlehem, Pennsylvania

Le-Wu Lu, Ph.D.
Professor
Department of Civil and Environmental Engineering
Lehigh University
Bethlehem, Pennsylvania

Unbonded post-tensioned precast concrete beam-column subassemblages have been studied in previous research and were found to be a promising seismic resistant structural system. The behavior of two six-story unbonded post-tensioned frames is studied using nonlinear push-over static analyses and time-history dynamic analyses. Two analytical models are developed for the analyses; the fiber model and the spring model. The results show that the behavior of unbonded post-tensioned precast frames, in particular, the strength, ductility, and self-centering capability, is more than adequate for severe earthquake loading.

Precast concrete structural systems for buildings are cost-efficient systems which provide high quality, and fast, easy erection on site. However, the research performed on precast concrete structural systems is limited compared to research on reinforced concrete systems. As a result, the U.S. model building codes include detailed seismic design provisions for cast-in-place reinforced concrete structural systems, but include only general provisions for the design of precast concrete structural systems.

In response to the recognized need for research on precast concrete systems for seismic regions, the PRESSS (Precast Seismic Structural Systems) research program was initiated in 1990.[1] The PRESSS research program is a coordinated program of analytical and experimental research intended to develop seismic resistant structural systems and seismic design provisions for precast concrete structures. The research described in this paper was performed as part of the PRESSS program.

This paper focuses on unbonded post-tensioned precast concrete frames. Prototype frames are discussed first. Then, the behavior of beam-column connections/subassemblages is discussed. Criteria are then proposed for the design of unbonded post-tensioned precast frames. The design of the prototype frames according to the design criteria is then discussed. Finally, the results of static and dynamic analyses of the prototype frames are presented and discussed.

SELECTION OF PROTOTYPE FRAMES

The prototype structures investigated in this paper are six-story office buildings. The layout of the lateral and gravity load frames of the prototype structures is shown in Fig. 1(a). An elevation view showing the story heights and precast concrete components is given in Fig. 1(b). The building layout is adopted from the layout suggested by Nakaki and Englekirk.[2]

The lateral load system is comprised of four unbonded post-tensioned precast frames, two for each direction, located on the perimeter of the plan. The lateral load resisting frames (prototype frames) also carry gravity loads. The floor system consists of 24 in. (610 mm) deep double tees running in the north-south direction of the building. The floor system is provided with a 2.5 in. (64 mm) thick cast-in-place concrete topping.

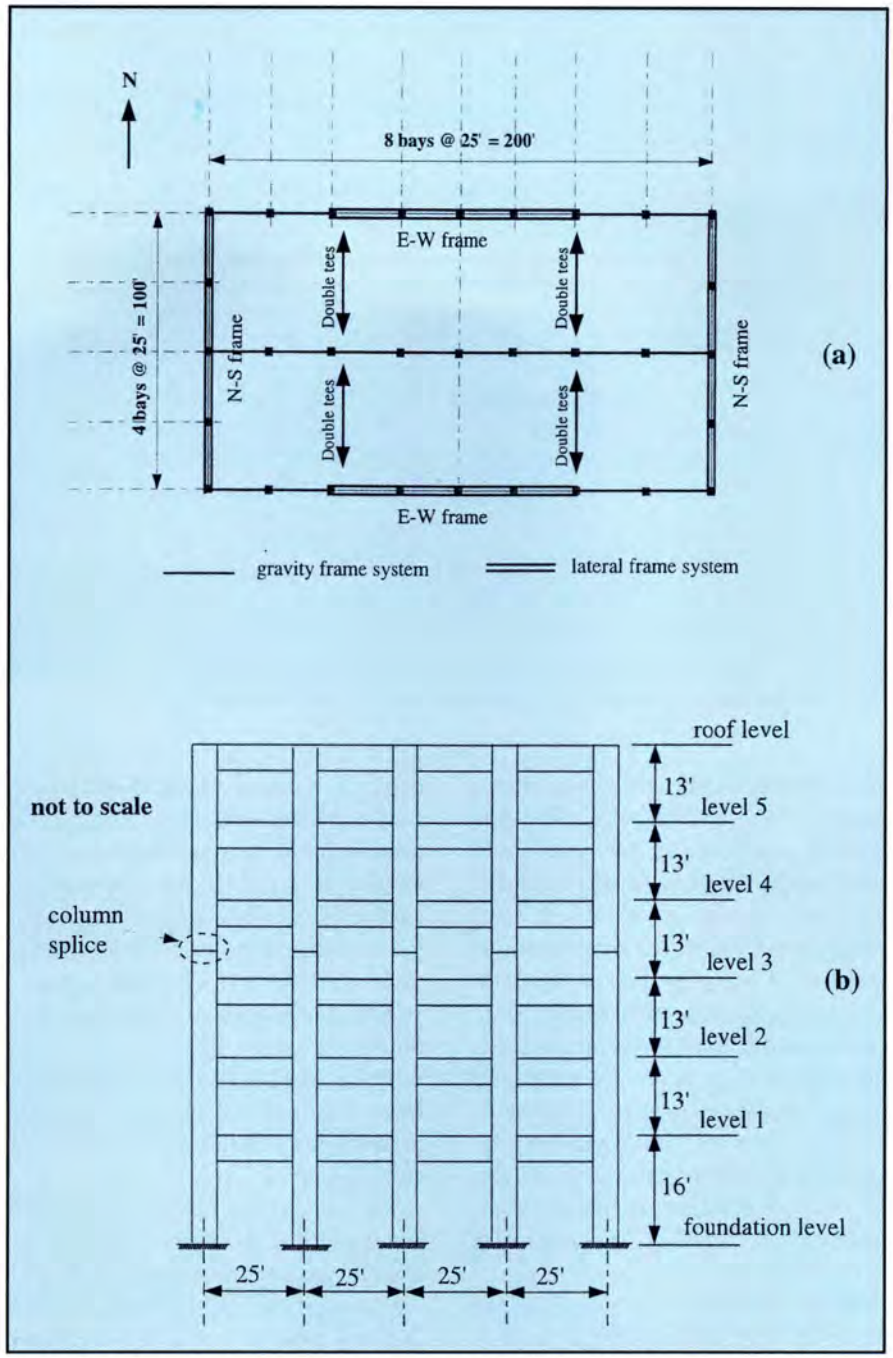

Fig. 1. Prototype frames: (a) layout of prototype building; (b) elevation view of prototype frames. **Note:** 1 ft = 305 mm.

SUBASSEMBLAGE BEHAVIOR AND MODELING

Unbonded post-tensioned precast concrete frames are designed as "ductile frames," in which the nonlinear/inelastic deformations occur only in the connections. Therefore, the frame behavior is controlled by the beam-column connection behavior. To investigate the beam-column connection behavior, a subassemblage is cut from the frame at the locations of hypothetical points of inflection located at midheight of the columns and midspan of the beams (see Fig. 2).

The subassemblage consists of connected beam and column segments with boundary conditions typical of beam-column subassemblage test specimens. The beam-column connection is considered to be the part of the beam adjacent to the column. The post-tensioning steel is unbonded through the column and for some distance through the beams on each side.

The flexural behavior of an unbonded post-tensioned beam-column connection is characterized by gap opening/closing at the beam-column interface upon loading/unloading. Unlike cast-in-place connections, the inelastic deformations are concentrated in the connection region where a "crack" already exists between the precast beam and column segments. In addition, because the post-tensioning steel is unbonded, additional flexural cracks do not form in the beam in the connection region.

The load-deflection behavior of the subassemblage is essentially nonlinear elastic as shown in Fig. 3. Although this behavior provides little energy dissipation, a frame utilizing this type of connection can be designed to return to its original position without residual displacement (self-centering)

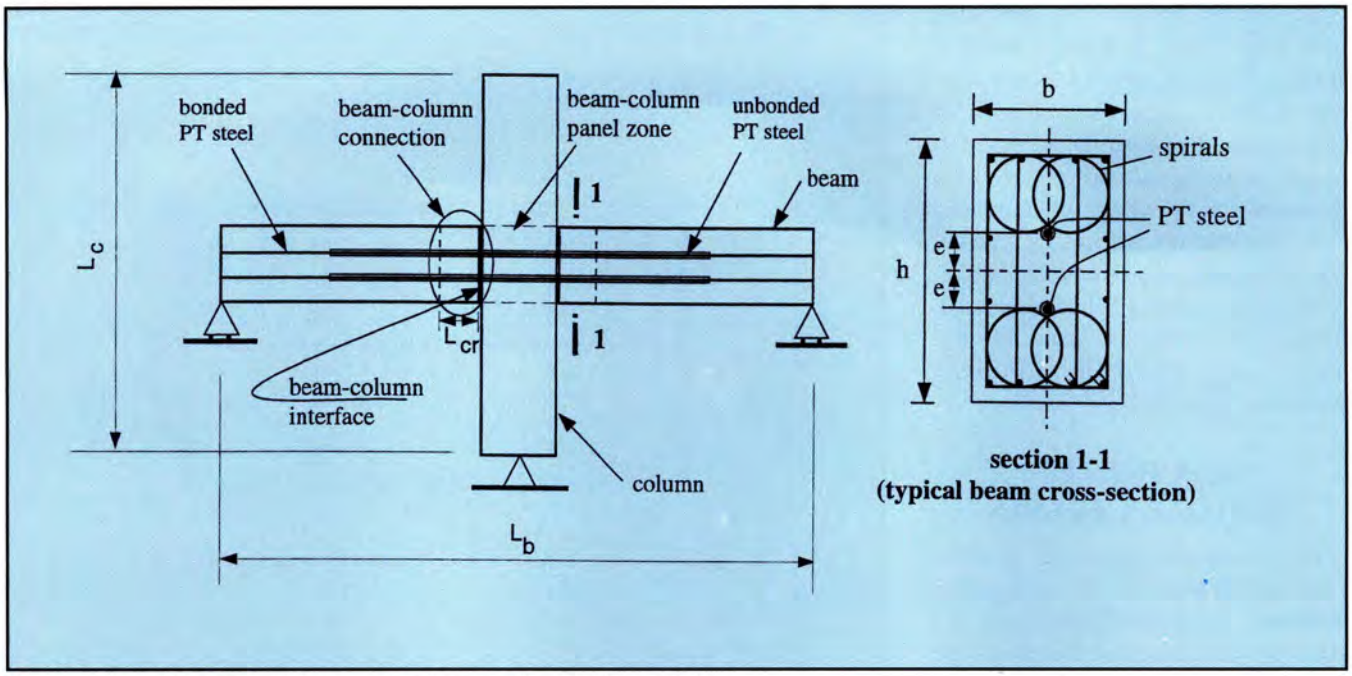

Fig. 2. Unbonded post-tensioned precast beam-column subassemblage.

and to retain its initial stiffness after a design level earthquake. The unbonded length of the post-tensioning steel can be designed to allow the displacement demand of the design level earthquake to be reached without yielding of the post-tensioning steel. Consequently, the prestressing force can be maintained through the loading/unloading cycles. A wide gap (crack) is expected at the beam-column interface, and the associated concrete compression strains near the gap are likely to be large. Therefore, spiral reinforcement (see Fig. 2) is necessary to confine the concrete.

Shear deformations occur in the beam-column subassemblage, including the beam-column panel zone. Shear deformations in the beams and columns should be kept in the elastic range. Moreover, shear slip at the beam-column interface should be prevented by providing an appropriate clamping force through the connection that is sufficient for all load conditions. Compared to a bonded post-tensioned connection, an unbonded post-tensioned connection maintains its initial clamping force through much larger levels of drift, because inelastic deformation of the post-tensioning steel is delayed.

Two analytical models have been developed for the beam-column subassemblage: the fiber model (FM), and the spring model (SM).[3,4] Fig. 4 shows the two models which use elements from the computer program DRAIN-2DX.[5]

Fig. 3. Nonlinear elastic load-deflection behavior.

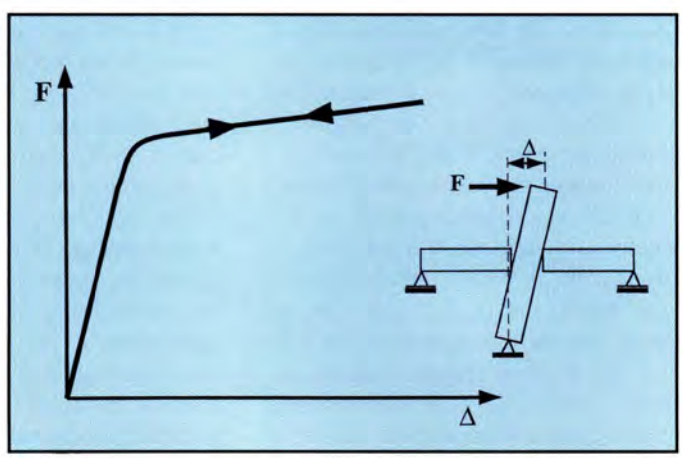

In the FM, the behavior of the concrete in the beam-column connection region is modeled using fiber beam-column elements. Other elements used in the FM include: (1) elastic beam-column elements to model parts of the beams and columns where only linear elastic deformations are expected to occur; (2) truss elements to model the unbonded post-tensioning steel; (3) a zero-length spring element to model the panel zone shear deformations; (4) rigid links and rigid end zones to model the axial and flexural deformations of the portions of the beams and columns within the panel zone, respectively; and (5) rigid links to tie the truss element end nodes to the adjacent fiber nodes at the locations of the post-tensioning steel anchorages.

In the SM, the nonlinear behavior of an unbonded post-tensioned precast beam-column connection is modeled using a zero-length rotational spring element, which replaces the fiber and truss elements in the FM. The SM is expected to give less accurate results than the FM. However, the hysteretic behavior of the SM can be directly controlled varying a factor (α_r), unlike the hysteretic behavior of the FM, which depends directly on the behavior of the concrete and steel fibers used to model the beam cross section. This feature of the SM is used in parametric studies of the dynamic response

of the prototype frames, as discussed later.

The FM and the SM are verified by comparing their behavior with the results of a test conducted at NIST on Specimen GPZ4.[6] Fig. 5(a) shows the experimentally determined hysteretic behavior of NIST Specimen GPZ4, plotted as lateral load versus lateral deflection. Figs. 5(b) and (c) show the hysteretic behavior of this specimen predicted by analysis using the FM and the SM, respectively.

Both models provide a good estimate of the hysteretic behavior of the test specimen. In particular, the initial stiffness and the strength are accurately predicted by both models. The hysteresis loops of the analytical models appeared to be narrower than the test results which indicates that the models underestimate the energy dissipation of the specimen.

BEHAVIOR OF BEAM-COLUMN CONNECTIONS

The moment-rotation behavior of an unbonded post-tensioned beam-column connection is characterized by several limit states, which are related to the stress-strain state of the concrete and the stress-strain state of the post-tensioning steel. The following discussion is based on studies of a large number of unbonded post-tensioned beam-column connections.[3,4]

Fig. 6 shows the typical moment-rotation behavior of a connection designed to have yielding of the post-tensioning steel before failure (crushing) of the confined concrete. Fig. 6 also shows a trilinear idealization of the moment-rotation behavior. Five limit states are identified.

State 1 is the decompression limit state. It represents the beginning of gap opening at the beam-column interface, when the concrete reaches zero stress at the extreme fiber of the beam. Increasing the moment beyond the decompression moment (M_{dec}) causes: (1) an initiation of gap opening and an increase in the length of the gap opening along the interface which results in geometric softening of the connection; and (2) an increase in the stress and strain in the concrete which eventually

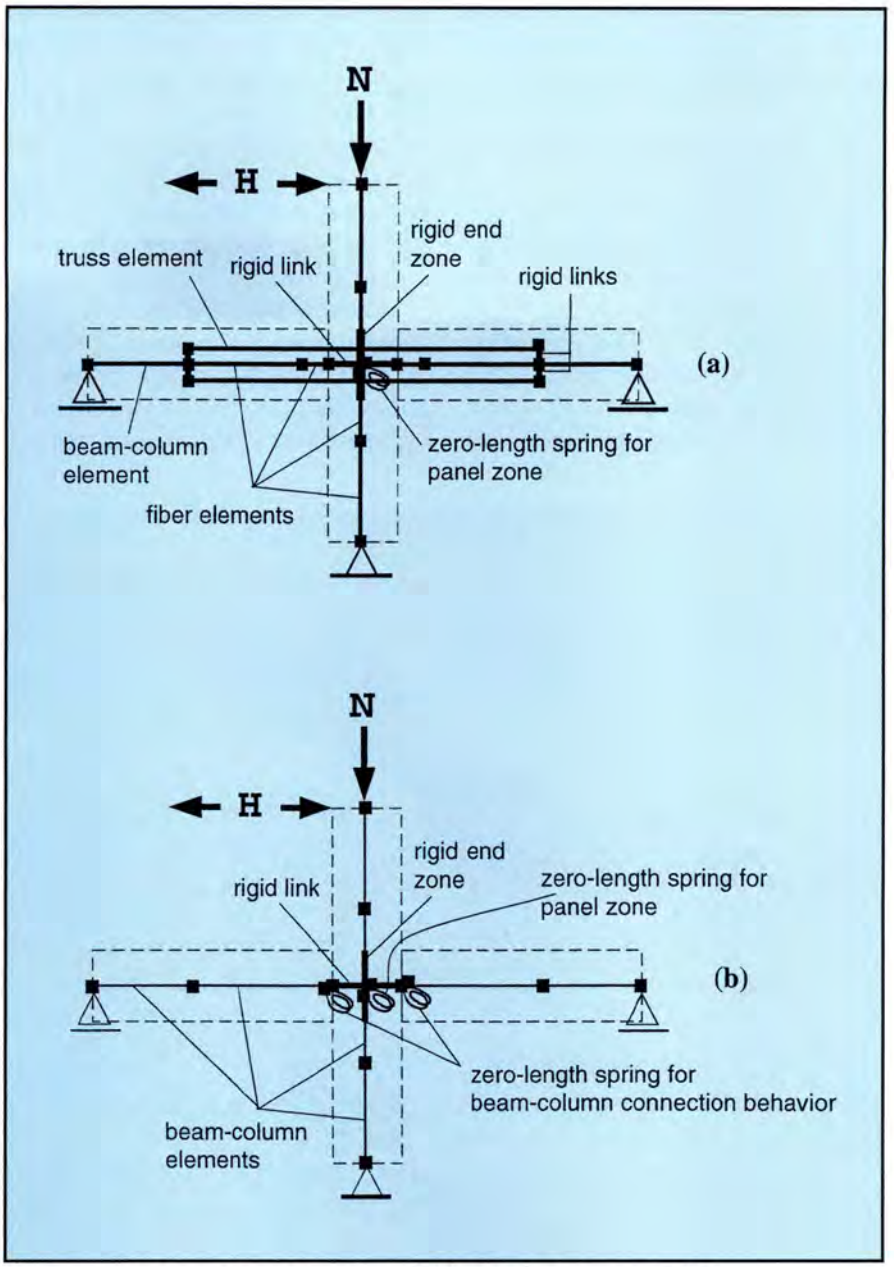

Fig. 4. Analytical models: (a) fiber model (FM); (b) spring model (SM).

results in concrete softening. Both of these effects gradually soften the moment-rotation behavior of the beam-column connection.

State 2 is the linear limit state (M_{ll},θ_{ll}). This is the state at which the moment-rotation behavior significantly deviates from the initially linear behavior and begins to soften dramatically. The linear limit is not well defined in terms of the stress-strain state of the concrete or the post-tensioning steel.

State 3 is the cover spalling limit state. This is the state at which the unconfined concrete cover spalls. At this state, a rapid decrease in the unconfined concrete stress takes place, causing a decrease in the slope of the beam moment-rotation relationship.

State 4 is the yield limit state (M_y,θ_y). This is the state at which the post-tensioning steel reaches the limit of proportionality (f_{pl}) on the post-tensioning steel stress-strain curve. The yield limit state is the upper bound on the elastic behavior of the beam-column connection. Beyond this state, the post-tensioning steel deforms inelastically, but the inelastic strain in the post-tensioning steel is small, because the inelastic strain is spread over the unbonded length.

State 5 is the ultimate limit state (M_{ult},θ_{ult}). This is the state when the strain in the extreme fiber of the con-

fined concrete reaches its ultimate strain (ε_{cu}) which is defined by fracture of the spiral reinforcement. A sudden failure is expected because a large volume of confined concrete will fail when the spirals fracture.

An idealized trilinear moment-rotation behavior for unbonded post-tensioned beam-column connections has been developed for use in the design of these connections. The idealization is based on approximate formulas for estimating the moment and rotation at three limit states, namely, the linear limit, the yield limit, and the ultimate limit states. The moment is calculated at the beam-column interface, while the rotation is calculated as the difference between the rotation at the column face and the rotation of the section (at a hypothetical point of inflection) at the midspan of the beam.

The derivation of the approximate formulas is based on several assumptions, the most important is that, in axial-flexural deformation, plane sections are assumed to remain plane after loading. Table 1 gives the approximate formulas used for the trilinear idealization. The detailed derivation of the approximate formulas can be found in the reports by El-Sheikh et al.[3,4]

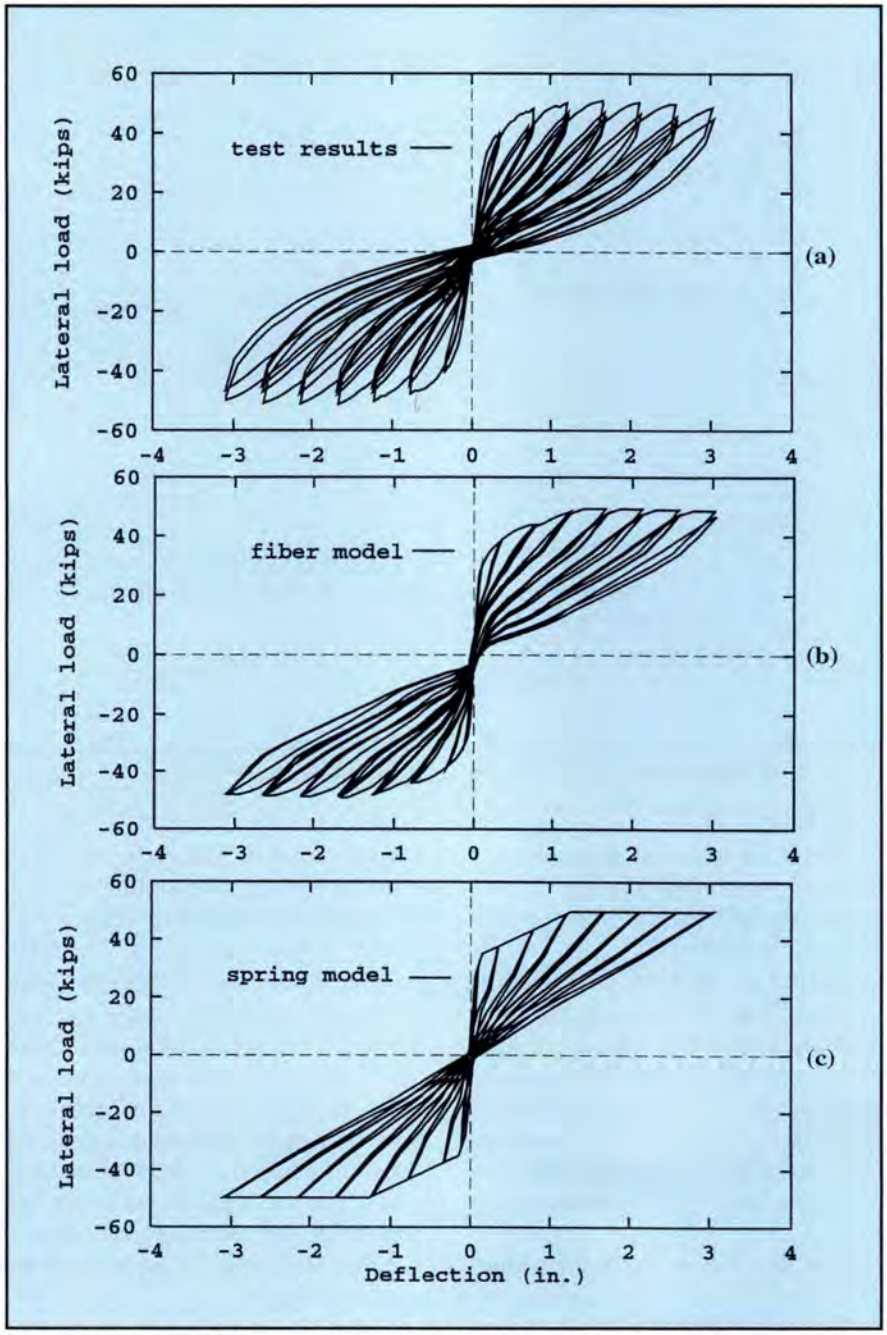

Fig. 5. Lateral load-deflection relationship for NIST Specimen GPZ4: (a) test results; (b) fiber model (FM); (c) spring model (SM). **Note:** 1 in. = 25.4 mm; 1 kip = 4.45 kN.

Estimation of the Linear Limit (M_{ll},θ_{ll}) — The linear limit moment (M_{ll}) is considered to be the smaller of two values; the first value accounts for concrete softening and the second value accounts for geometric softening due to gap opening. The first value of M_{ll} is the moment calculated by including the concrete cover, treating all the concrete as unconfined, assuming the extreme fiber strain of the concrete is 0.003, and assuming the force in the post-tensioning steel is the initial force (neglecting post-tensioning steel elongation). The second value of M_{ll} considers the opening of the gap at the beam-column interface. Typically, the effect of the gap opening on the slope of the moment-rotation curve is small until the gap opening length has propagated beyond the section centroid.[7]

Based upon studies of numerous beam-column connections using the fiber model, in which softening was not significant until the gap opening length propagated over 75 percent of the section depth, the linear limit moment which accounts for gap opening was selected to be $2.5M_{dec}$. The linear limit rotation (θ_{ll}) is calculated assuming the beam is uncracked, i.e., based on the initial stiffness of the moment-rotation curve.

Estimation of the Yield Limit (M_y,θ_y) — The estimation is based on several assumptions, the most important are: (1) the elastic flexural deformations over the length of the beam are negligible, since the rotation due to gap opening and deformation of the concrete near the beam-column interface is dominant, and the elastic deformations of the rest of the beam are small, (2) the center of rotation at the beam-column interface is at the neutral axis, and (3) the cover concrete has spalled.

Estimation of the Ultimate Limit (M_{ult},θ_{ult}) — Referring to Fig. 6, the beam ultimate moment (M_{ult}) is assumed equal to the yield moment (M_y). The main factors affecting the ultimate rotation capacity (θ_{ult}) are the ultimate concrete strain (ε_{cu}) and the

failure length of the confined concrete adjacent to the beam-column interface (L_{cr}) shown in Fig. 2. L_{cr} can be estimated from the dimensions of the confined concrete in compression in the beam-column connection at the ultimate limit. In this study, L_{cr} is taken as the minimum of the confined concrete width (b'') and two times the stress block depth ($2a''$). The curvature is assumed constant over L_{cr} and the elastic deformations over the remaining length of the beam are neglected.

PROPOSED DESIGN APPROACH

A proposed design approach, based on the equivalent lateral force procedure of the NEHRP seismic design provisions[8] is described in this section. To provide sufficient ductility, a frame is designed so the failure mechanism is a beam sway mechanism, where hinges form at the beam-column connections and at the bases of the columns. A capacity design concept is used to ensure that the remainder of the frame will remain linear elastic.

The proposed seismic design approach considers two levels of earthquake ground motion, the design level and the survival level. The design level ground motion is chosen to be the design basis ground motion of the 1991 and 1994 editions of the NEHRP provisions[8] with a 90 percent probability of not being exceeded in 50 years, corresponding approximately to a 500-year return period. The survival level ground motion is assumed to have a 90 percent probability of not being exceeded in 250 years, corresponding approximately to a 2500-year return period. The survival level ground motion is taken to be 2.5 times the NEHRP design basis ground motion.

According to the proposed design approach, the design level ground motion may cause only minor, easily repaired damage to both structural and nonstructural components, while the survival level ground motion may cause damage to the structure that cannot be repaired, but should not cause the structure to collapse.

The nonlinear behavior of a well-designed unbonded post-tensioned precast frame is controlled by the moment-rotation behavior of the beam-column connections. Therefore, the lateral load behavior of the frame is idealized using a trilinear base shear-roof displacement relationship based on the trilinear idealization of the moment-rotation behavior. The idealized base shear-roof displacement behavior is shown in Fig. 7, where three regions can be characterized. The first region is essentially linear elastic. The second region is characterized by a significantly reduced stiffness. The third region is a yielding plateau with essentially zero slope.

Three limit states are shown on the trilinear idealization of the frame behavior. The linear limit state (V_{ll},Δ_{ll}) corresponds to the effective linear limit of the frame which is controlled by the linear limit of the beam-column connections. The yield limit state (V_y,Δ_y) corresponds to an effective yield limit of the frame, when stresses in the post-tensioning steel in the beam-column connections reach the limit of proportionality of the steel.

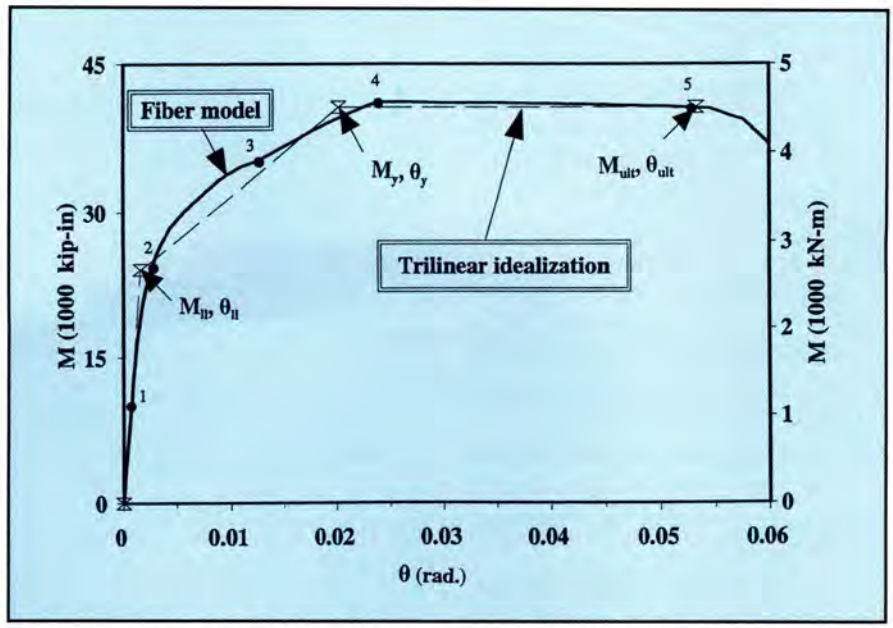

Fig. 6. Moment-rotation behavior of unbonded post-tensioned connection predicted by FM and proposed trilinear idealization. **Note:** 1 in. = 25.4 mm; 1 kip = 4.45 kN.

Table 1. Approximate formulas for moment-rotation behavior of beam-column connections.

Limit state	Moment	Rotation
Linear limit state	Smaller of the following: $M_{ll} = 0.50 f_{pi} A_p h \left(1 - \frac{f_{ci}/f_c'}{0.85}\right)$; $M_{ll} = 0.42 f_{pi} A_p h$	Smaller of the following: $\theta_{ll} = \frac{3 L_{bc} f_{ci}}{2 h E_c}\left(1 - \frac{f_{ci}/f_c'}{0.85}\right)$; $\theta_{ll} = \frac{2.5 L_{bc} f_{ci}}{2 h E_c}$
Yield limit state *	$M_y = 0.5 f_{pi} A_p (h'' - a'')$; $a'' = \frac{c_1}{\alpha}\frac{f_{ci}/f_{cc}'}{f_{pi}/f_{pu}}\frac{b}{b''}h$	$\theta_y = \frac{(f_{pi} - f_{pi}) L_{pu}}{(0.5h'' - a''/\beta) E_p}$
Ultimate limit state	$M_{ult} = M_y$	$\theta_{ult} = \frac{\varepsilon_{cu}\beta}{a''} L_{cr}$

Note: Notation is given in the Appendix.

* Approximate formulas for yield limit state are limited to interior beam-column connections and to exterior beam-column connections with concentric post-tensioning steel.

The ultimate limit state (V_{ult},Δ_{ult}) corresponds to failure of confined concrete in the beam-column connections.

Three base shear levels are defined in Fig. 7: (1) elastic base shear (V_{el}); (2) design base shear (V_{des}); and (3) survival base shear (V_{sur}). The design base shear (V_{des}) corresponds to elastic response to the design level ground motion. The survival base shear (V_{sur}) corresponds to elastic response to the survival level ground motion and is taken as 2.5 times V_{des}. The elastic base shear (V_{el}) is the reduced base shear demand used in design, and is taken as V_{des} divided by a response modification factor (R).

The behavior of an unbonded post-tensioned precast frame (see Fig. 7) is not easily predicted after the beam-column connections reach their linear limit, because the distribution of internal forces and deformations in the frame differs from the linear elastic distribution. This redistribution results in significant variations in the ductility demands among the beam-column connections, and the ductility demands on the beam-column connections are expected to be larger than the expected frame ductility demands.

The NEHRP[8] equivalent lateral force procedure idealizes seismic loading as static lateral forces. The force levels prescribed by the NEHRP design provisions are significantly lower than required to ensure a linear elastic response, as nonlinear behavior is allowed for economic reasons. The response modification factors (R) defined in NEHRP, are used to obtain reduced force levels (shown as V_{el} in Fig. 7) from the forces corresponding to linear elastic response to the design basis ground motion. The unbonded post-tensioned precast frame system is considered to be a special moment resisting frame system with ductile connections, and the corresponding value of $R = 8$ is used in design.

The proposed design approach uses the NEHRP equivalent lateral force procedure to determine the member forces and deformations. Design criteria for the flexural behavior of the beam-column connections are given below. Fig. 8 shows the idealized trilinear moment-rotation relationship for the beam-column connection, together with the notation used to describe the design criteria. The design approach has three sets of criteria related to the three limits of the trilinear idealization.

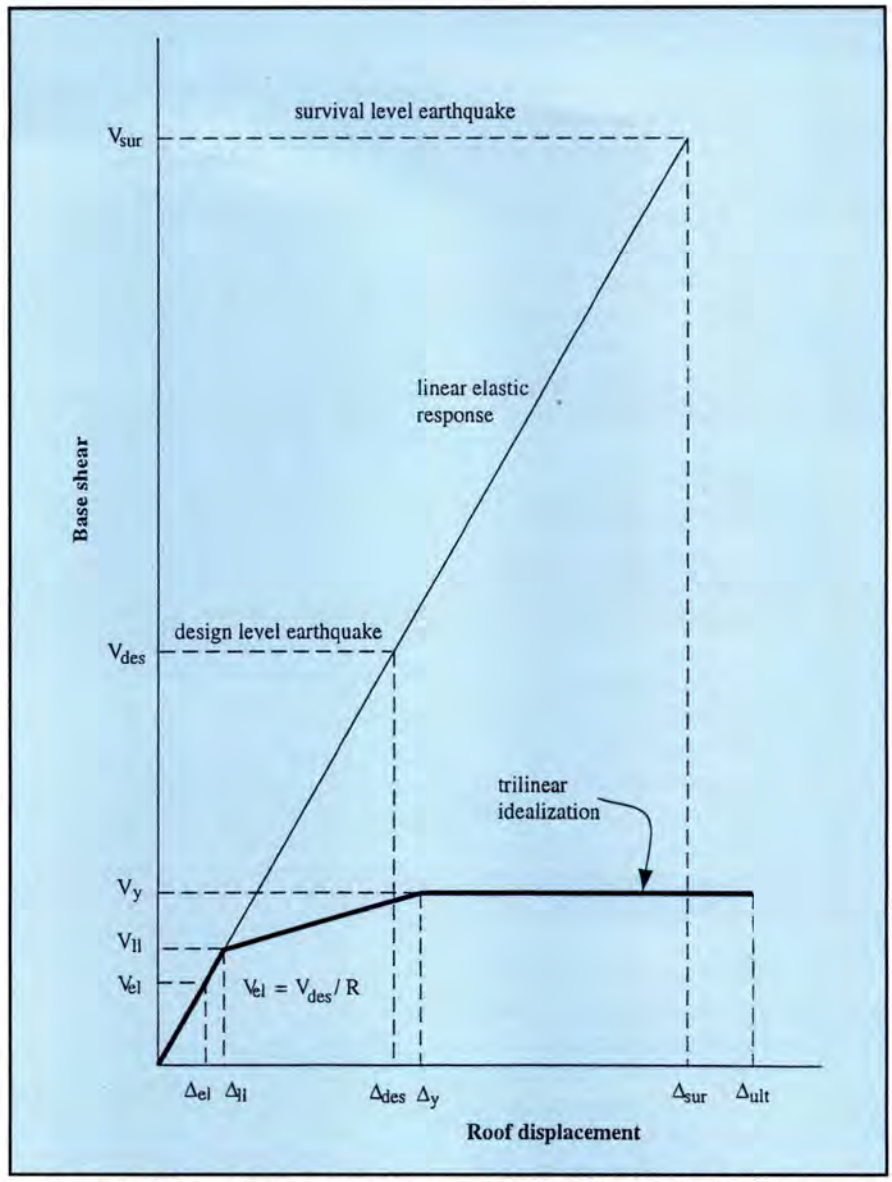

Fig. 7. Expected base shear-roof displacement behavior of unbonded post-tensioned precast frame.

Linear Limit State Criteria — The linear limit criteria are used to ensure that the connection has sufficient stiffness. The response of the beam-column connection up to the linear limit is essentially linear elastic. The linear limit criteria are defined in terms of both moment and rotation. The criterion for moment is:

$$M_{el} \leq M_{ll} \qquad (1)$$

where M_{el} is the beam-column connection bending moment demand for the reduced level of earthquake loading (shown as V_{el} in Fig. 7), estimated using linear elastic analysis of the frame under NEHRP[8] equivalent lateral forces (and factored gravity loads).

The linear limit criterion for rotation is related to the allowable story drift given in the NEHRP provisions.[8] Assuming that the story drift is mainly caused by the beam-column connection rotation, the criterion is written as follows:

$$\theta_{el} \leq \theta_{all}/C_d \qquad (2)$$

where

θ_{el} = beam-column connection rotation demand for the reduced level of earthquake loading, estimated using linear elastic analysis under NEHRP[8] equivalent lateral forces

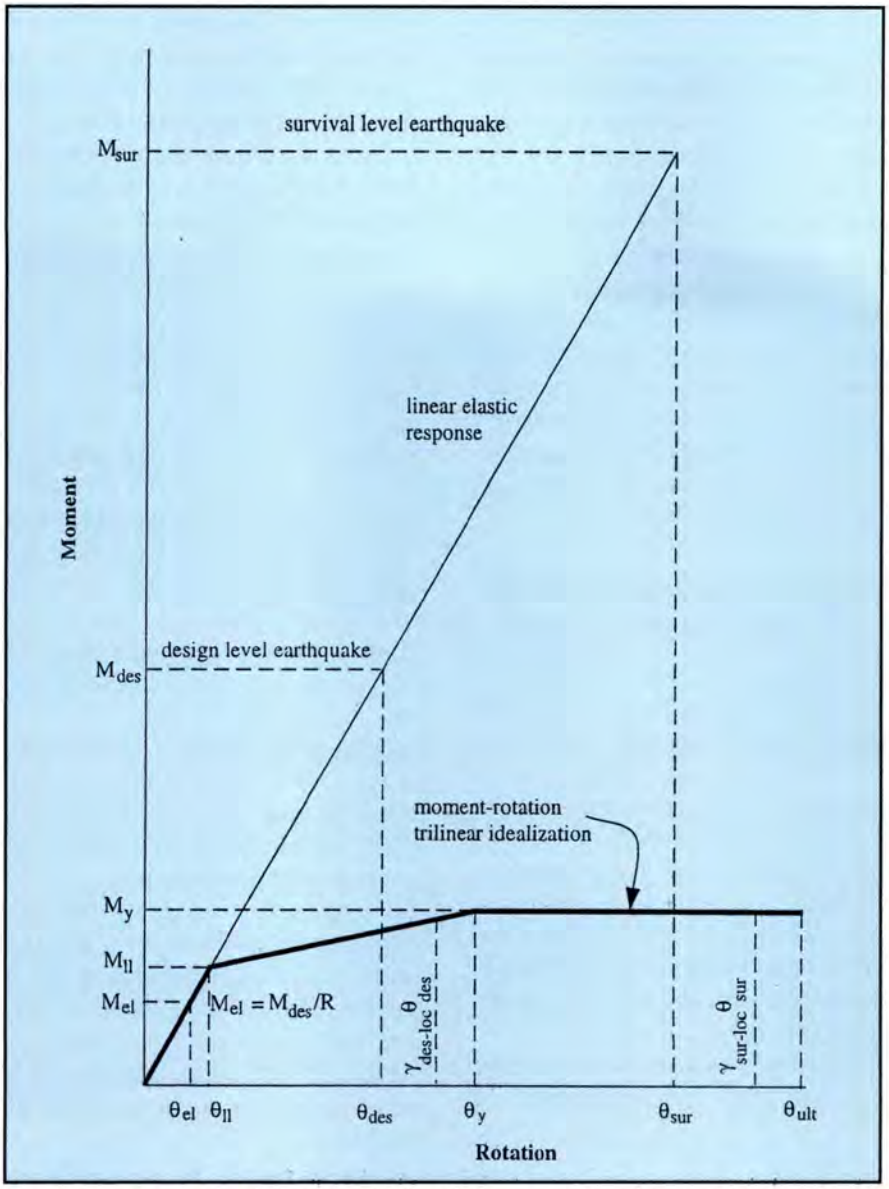

Fig. 8. Moment-rotation behavior of unbonded post-tensioned precast beam-column connection.

θ_{all} = allowable rotation which is taken as the allowable story drift of the NEHRP provisions[8]

C_d = NEHRP inelastic deflection amplification factor

The purpose of this criterion is to impose frame stiffness requirements on an unbonded post-tensioned precast frame similar to those imposed on other systems by the NEHRP provisions.[8]

Yield Limit State Criteria— The yield limit is related to the strength and deformability of the beam-column connection. The demands from the design level ground motion are compared to the yield limit to ensure that the beam-column connection has adequate strength and deformability. The yield limit criteria are defined in terms of both moment and rotation. The criterion for moment is similar to the flexural strength design criterion for cast-in-place reinforced concrete. This criterion requires the beam-column connection bending moment demand corresponding to the NEHRP[8] equivalent lateral forces to be less than or equal to the factored connection bending moment capacity:

$$M_{el} \le \phi M_y \qquad (3)$$

where ϕ is the flexural capacity reduction factor in accordance with the ACI 318 Code.[9]

The yield limit criterion for rotation is used to ensure sufficient elastic deformability in the connection. The yield rotation is used, so that the post-tensioning steel in the connection can remain elastic under the design level ground motion. Avoiding yield of the post-tensioning steel permits the frame to survive the design level ground motion with little or no structural damage. The criterion is:

$$\gamma_{des\text{-}loc}\,\theta_{des} \le \theta_y \qquad (4)$$

where

$\gamma_{des\text{-}loc}$ = local ductility demand factor for the design level ground motion, greater than unity

$\theta_{des} = (M_{des}/M_{el})\,\theta_{el} = R\theta_{el}$ = beam-column connection rotation for the design level of earthquake loading, estimated from θ_{el} using an equal displacement assumption

The product $\gamma_{des\text{-}loc}\theta_{des}$ is an estimate of the rotation demand on the connection under the design level ground motion. The factor $\gamma_{des\text{-}loc}$ accounts for uncertainty in the ductility demand on the beam-column connection, as discussed later.

Ultimate Limit State Criterion — The ultimate limit is used to ensure sufficient inelastic deformability in the connection. The ultimate limit criterion is established with respect to the survival level ground motion. This criterion defines the inelastic deformability required to prevent failure of the spiral confined concrete in the beam-column connections which could lead to sudden collapse of the frame. The criterion for rotation is:

$$\gamma_{sur\text{-}loc}\,\theta_{sur} \le \theta_{ult} \qquad (5)$$

where

$\gamma_{sur\text{-}loc}$ = local ductility demand factor for survival level ground motion, greater than unity

$\theta_{sur} = (M_{sur}/M_{el})\,\theta_{el} = 2.5R\,\theta_{el}$ = beam-column connection rotation for the survival level of earthquake loading, estimated from θ_{el} using an equal displacement assumption, when the intensity of the survival level ground motion is taken as 2.5 times the intensity of the design level ground motion

The product $\gamma_{sur\text{-}loc}\,\theta_{sur}$ is an estimate of the rotation demand on the connection under the survival level ground motion. The factor $\gamma_{sur\text{-}loc}$ accounts for uncertainty in the ductility demand on the beam-column connection, as discussed later.

Flexural capacity design criteria are adopted for the frame members and connections intended to remain elastic under all loading conditions.[3,4] Columns (except at their bases) and beams (except at their ends) should possess flexural strength in excess of the bending moments corresponding to the strength of the relevant beam-column connections. Similarly, shear capacity design criteria are adopted to avoid excessive shear deformations and stiffness softening due to shear.[3,4] Shear slip at the beam-column interface should be avoided by providing appropriate shear friction resistance at the interface.

DESIGN OF PROTOTYPE FRAMES

Four prototype frames were designed using the proposed design approach.[3,4] Only two frames, Frame 1 and Frame 4 are discussed in this paper. Frame 1 and Frame 4 were designed for high and moderate seismicity zones, respectively. The 1991 edition of the NEHRP provisions was used to design the prototype frames, which were designed before the 1994 edition was published in May 1995.

The frames were designed as special moment resisting frames with R equal to 8, C_d equal to 5.5, and θ_{all} equal to 1.5 percent. The frames were designed to satisfy the requirements of both the north-south frames and the east-west frames of the prototype building. Table 2 shows the main parameters that influence the base shear demand according to NEHRP.[8]

Using the proposed design approach outlined above, connections, beams, and columns are designed for both frames. The local ductility demand factors were set to unity in the design. Table 3 summarizes the beam and column cross-sectional dimensions for the two prototype frames.

PUSH-OVER ANALYSES OF PROTOTYPE FRAMES

Nonlinear push-over static analyses of the prototype frames were conducted using a triangular distribution of lateral forces, similar to the NEHRP[8] lateral force distribution. The analyses included dead load and 25 percent of the design live load as gravity loads. All frames were analyzed as north-south frames which have less gravity load than the east-west frames. These analyses are called low gravity load (LGL) cases.

Frame 4 was also analyzed as an east-west frame (as a high gravity load (HGL) case). The frames were pushed to a target roof displacement equal to 40 in. (1020 mm), which corresponds to 4.1 percent roof drift. The static analyses used both the fiber model (FM) and the spring model (SM) for the frames. These models are similar to the beam-column subassemblage models, shown in Fig. 4.

Table 4 summarizes three levels of estimated roof displacement corresponding to the elastic (reduced), design, and survival levels of earthquake loading for the FM of each prototype frame. Table 4 also shows the calculated fundamental period of the prototype frames and the period used in design based on the 1991 edition of the NEHRP provisions.[8]

Fig. 9 shows the frame base shear (V) versus roof displacement (Δ) for both the FM and the SM of Frame 1. Fig. 10 shows V versus Δ for the FM of Frame 4. The three levels of roof displacement corresponding to the elastic (reduced), design, and survival levels of earthquake loading, given in Table 4, are shown in Figs. 9 and 10. Also shown in the figures are the range of roof displacements at which yielding of columns at the base initiates, and the range of roof displacements at which yielding of the post-tensioning steel initiates, from the FM results.

Comparing the SM to the FM in Fig. 9, the SM results are in a good agreement with those of the FM. The push-over behavior of the frames is discussed in the following paragraphs, starting with comparisons of the behavior with the proposed design requirements.

Elastic Level Requirements — All the elastic level requirements are satisfied in both frames. Spalling of the concrete cover, yielding of the steel reinforcement, and softening of the beam-column connections do not occur before the elastic (reduced) level base shear (V_{el}) is reached. Therefore, the behavior is essentially linear elastic up to the elastic level base shear. In addition, the drift limits are satisfied.

Design Level Requirements — Softening of the base shear-roof displacement behavior was observed, as expected, between the elastic level and the design level. The two main sources

Table 2. Description of the two prototype frames.

	Seismic zone	Soil conditions	Period used in design
Frame 1	High seismicity ($A_a = A_v = 0.4$)	Medium soil ($S = 1.2$) (Soil type S_2)	$T = T_a = 0.82$ seconds
Frame 4	Moderate seismicity ($A_a = A_v = 0.1$)	Medium soil ($S = 1.2$) (Soil type S_2)	$T = C_a T_a = 1.38$ seconds

A_a, A_v, T_a, C_a, S, and soil types are defined in the 1991 edition of NEHRP.[8]

Table 3. Member dimensions.

Member	Frame 1	Frame 4
All columns, in. (mm)	28 x 38 (710 x 970)	22 x 26 (560 x 660)
Sixth floor (roof) beams, in. (mm)	24 x 26 (610 x 660)	16 x 20 (410 x 510)
Fourth and fifth floor beams, in. (mm)	24 x 34 (610 x 860)	16 x 24 (410 x 610)
Second and third floor beams, in. (mm)	24 x 40 (610 x 1020)	18 x 26 (460 x 660)
First floor beams, in. (mm)	24 x 42 (610 x 1070)	18 x 26 (460 x 660)

of the softening are: (1) softening of the beam-column connections after the linear limit is reached; and (2) yielding of columns at the base of the frames. Concrete cover spalling takes place at some of the beam-column connections and column bases.

The contribution of column base yielding to the softening of the frame is expected. The first-story columns were designed to behave as conventional reinforced concrete columns. They were designed to yield at the base at a bending moment close to the moment demand for the reduced level of earthquake loading (V_{el}). In the frame analytical models, the first-story columns were modeled using beam-column elements with the possibility of yielding at the base and considering axial force-moment interaction. The columns were fixed at the base in the models.

Most of the softening of the frames observed in Figs. 9 and 10 is due to the softening of the beam-column connections after the linear limit is reached. The figures show the range of roof displacements at which yielding of columns at the base initiates. The beam-column connections reach their linear limit at similar or slightly larger values of roof displacement.

A significant redistribution of internal forces (compared to the linear elastic distribution) occurs due to softening of the frame. This causes yielding of the post-tensioning steel to occur over a wide range of roof displacement values. In general, the sequence of yielding of the post-tensioning steel progresses from the lower floors to the upper floors.

According to the yield limit state design criteria, yielding of the post-tensioning steel should not occur before the design level roof displacement (Δ_{des}) is reached. This criterion is not satisfied for Frame 1 (designed for high seismicity regions), but is satisfied for Frame 4 (designed for moderate seismicity regions). As discussed earlier, local ductility demand factors ($\gamma_{des\text{-}loc}$) are needed to amplify the design ductility demands on the beam-column connections, so that under the design level ground motions the post-tensioning steel will not yield before the design level roof displacement

Table 4. Roof displacements estimated in design and fundamental periods based on the fiber model.

Parameter	Frame 1	Frame 4
Δ_{el}, in. (mm)	1.62 (41)	1.38 (35)
Δ_{des}, in. (mm)	13.0 (330)	11.0 (279)
Δ_{sur}, in. (mm)	32.4 (823)	27.6 (701)
T	1.12 seconds	2.48 seconds
T used in design	0.82 seconds	1.38 seconds

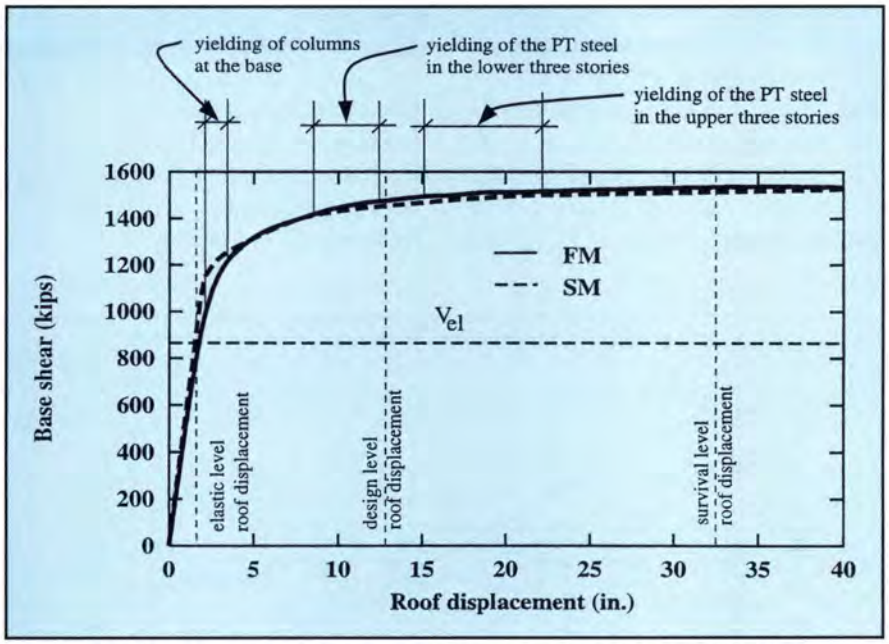

Fig. 9. Base shear vs. roof displacement of Frame 1, using the FM and the SM.
Note: 1 in. = 25.4 mm; 1 kip = 4.45 kN.

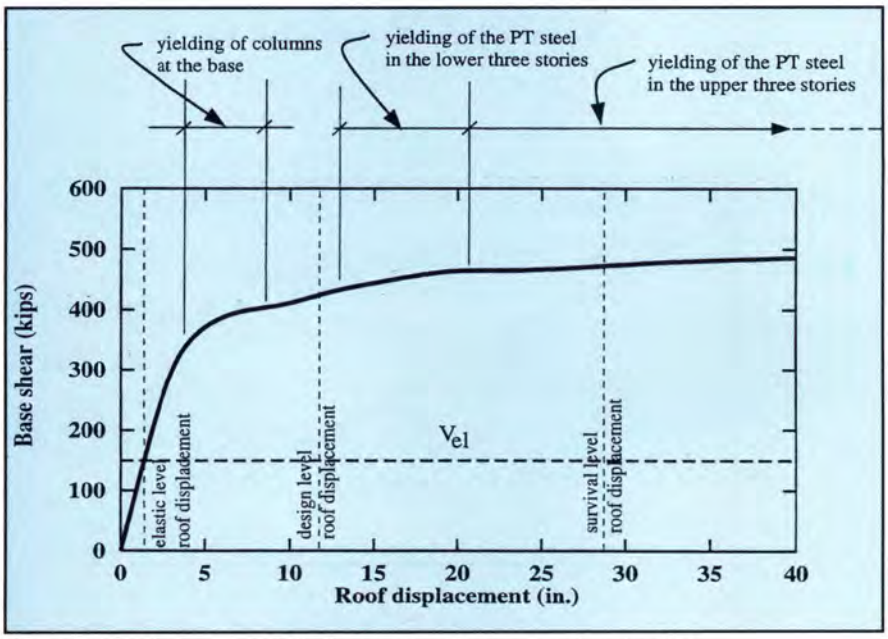

Fig. 10. Base shear vs. roof displacement of Frame 4, using the FM.
Note: 1 in. = 25.4 mm; 1 kip = 4.45 kN.

(Δ_{des}) is reached. Local ductility demand factors are discussed below.

Survival Level Requirements — According to the ultimate limit state design criterion, up to the survival level roof displacement, the confined concrete strain should not exceed the ultimate strain for the confined concrete (ε_{cu}) to avoid failure of concrete due to fracture of the spiral confining steel in the beam-column connections. The prototype frames did not experience this type of failure because the spirals in the prototype frames were overdesigned. As discussed earlier, local ductility demand factors ($\gamma_{sur\text{-}loc}$) are needed to amplify the beam-column design ductility demands for the survival level ground motions.

Local Ductility Demand Factors — The static analysis results[3,4] show that the required values of $\gamma_{des\text{-}loc}$ and $\gamma_{sur\text{-}loc}$ decrease as the contribution of gravity load to the beam-column connection design moment demand increases. The gravity load contribution to the design moment leads to an overdesign of the moment capacity of the beam-column connection that reduces the ductility demand. The gravity load contribution can be estimated as the ratio between the bending moment demand due to gravity loads and the total elastic bending moment demand including both gravity and lateral loads at the connection under consideration. Therefore, $\gamma_{des\text{-}loc}$ and $\gamma_{sur\text{-}loc}$ are larger for frames designed for high seismicity regions as compared to frames designed for moderate seismicity regions. Fig. 11 provides local ductility demand factors calculated from the static analysis results[3,4] for Frames 1, 2, 3, and 4.

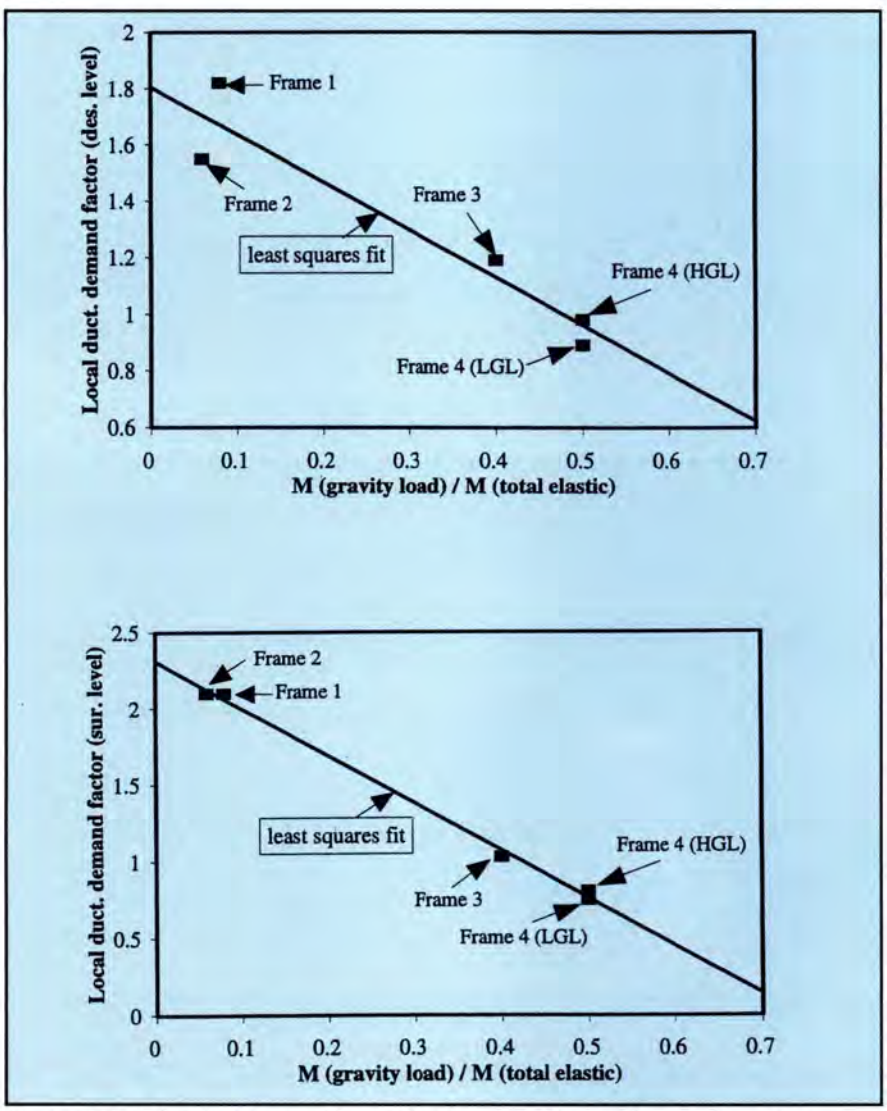

Fig. 11. Local ductility demand factors for design and survival ground motions.

Beam Elongation — One of the issues to be considered in the design of an unbonded post-tensioned precast concrete frame is the apparent elongation of the beams due to gap opening in the beam-column connections. As the lateral drift of the frame increases, the gap opening length and width increase at the beam-column interface and, accordingly, the centroidal axis of the beam measured from column face to column face elongates. The FM was used to study the beam elongation, and for the prototype frames the elongation was found to range between 1.5 to 2.5 percent of the beam height (h), for each beam span (L_b), as the roof drift reached 4.0 percent.

Two factors affect the elongation of the beams: foundation restraint on the columns; and relative beam elongations between adjacent floors. The effect of the foundation restraint is dominant for the lower floor beams. The effect of relative beam elongations between adjacent floors is not easily predicted.

The restraint of the beam elongation in the frame introduces a set of self-equilibrating forces in the frame, including forces at the foundation level. The beam-column connections and beams are subjected to additional axial forces, while the columns are subjected to secondary shear forces and bending moments. The axial forces in the beams are usually maximum at the first floor. The secondary shears and moments in the columns are proportional to their distance from the column at the center of the frame.

The effect of these axial forces in the beams is as follows: (1) the axial compression forces increase the bending moment capacity, increase the yield rotation, and decrease the ultimate rotation of the beam-column connections; and (2) the axial tension forces decrease the bending moment capacity, decrease the yield rotation, and increase ultimate rotation of the beam-column connections. The beam elongation effects should be considered in design. For example, the increase in the beam-column connection bending moment capacity was observed to be as large as 25 percent.

TIME-HISTORY DYNAMIC ANALYSES OF FRAME 1

The results of nonlinear time-history dynamic analyses of prototype Frame 1 are described in this section. The frame is analyzed for design and survival level earthquake ground motions. Natural recorded and artificially generated ground motions for different soil conditions (stiff/rock, medium, and soft soil) were used in the dynamic analyses. Table 5 summarizes the main characteristics of these ground motions, scaled to a peak ground acceleration (PGA) of 1.0*g*. Damping of the prototype frames is modeled as mass and stiffness proportional viscous damping, with a specified damping ratio of 3.0 percent for the first and third modes, and resulting damping ratios of 2.2 percent for the second mode, and 4.3 percent for the fourth mode.

Roof Displacement — The roof lateral displacement is representative of the overall frame displacement response. Fig. 12 shows time-histories of the lateral displacement of the roof and the second and fourth floor levels of Frame 1 during the NEW ground motion scaled to a peak ground acceleration of 0.4*g* to represent a design level ground motion. The dashed horizontal lines shown in Fig. 12 indicate the roof displacement for the design level ground motion estimated in design (Table 4). Fig. 12 shows that the roof displacement obtained from the dynamic analysis does not exceed the roof displacement estimated in design. Fig. 12 also shows that, at the time of the displacement peaks, the second and fourth floor displacements are generally in phase with the roof displacements.

Maximum Roof Displacement — The maximum roof displacement values obtained from the dynamic analyses of Frame 1 are tabulated in Table 6, where the corresponding roof drift values (the roof displacement divided by the total frame height) are also given. Fig. 13 compares the roof displacements obtained from the dynamic analyses (shown as discrete points), and the estimated roof displacements based on an equal displacement assumption (shown as an inclined solid line). The roof displacements are shown as a function of peak ground acceleration (PGA). Three symbols represent the dynamic analysis results for the three soil conditions (stiff/rock, medium, and soft soil).

Table 5. Properties of selected ground motions scaled to 1.0*g*.

Site soil condition	Earthquake		Earthquake/station name (year)	Peak ground acceleration (*g*)	Peak ground velocity (in./second)
	No.	Record			
Rock or stiff	1	ELC	El Centro/El Centro (1940)	1.00	43.6
	2	PRE	Loma Prieta/Presidio (1989)	1.00	66.3
	3	GST	Power spectrum based generated ground motion	1.00	77.8
	4	STF	SEAOC spectrum compatible generated ground motion	1.00	60.6
Medium	5	ORI	San Fernando/Orion (1971)	1.00	45.9
	6	HOL	Loma Prieta/Hollister (1989)	1.00	67.4
	7	YER	Landers/Yermo (1992)	1.00	82.5
	8	NEW	Northridge/Newhall (1994)	1.00	64.0
	9	SYL	Northridge/Sylmar (1994)	1.00	60.4
	10	GME	Power spectrum based generated ground motion	1.00	104
	11	MED	SEAOC spectrum compatible generated ground motion	1.00	107
Soft	12	FOS	Loma Prieta/Foster City (1989)	1.00	62.8
	13	TRE	Loma Prieta/Treasure Island (1989)	1.00	82.3
	14	GSO	Power spectrum based generated ground motion	1.00	147
	15	SOF	SEAOC spectrum compatible generated ground motion	1.00	80.4

Note: 1 in. = 25.4 mm.

As shown in Fig. 13, all of the roof displacements from the dynamic analyses for cases with stiff/rock soil conditions are conservatively estimated using the equal displacement assumption. For cases with medium soil conditions, the average of the roof displacements from the dynamic analyses are conservatively estimated. All of the roof displacements from dynamic analysis for cases with soft soil conditions exceed the estimated roof displacements.

Implications for Design — Fig. 13 shows that the maximum roof displacement values obtained from the dynamic analyses often exceed the estimated roof displacements, especially for design level ground motions on soft soil conditions and survival level ground motions on medium or soft soil conditions. When the estimated roof displacements are exceeded, the ductility demands on beam-column connections are larger than expected, and adequate ductility capacity may not be available. Moreover, the maximum roof displacements during survival level ground motions on medium and soft soil conditions are unacceptably large.

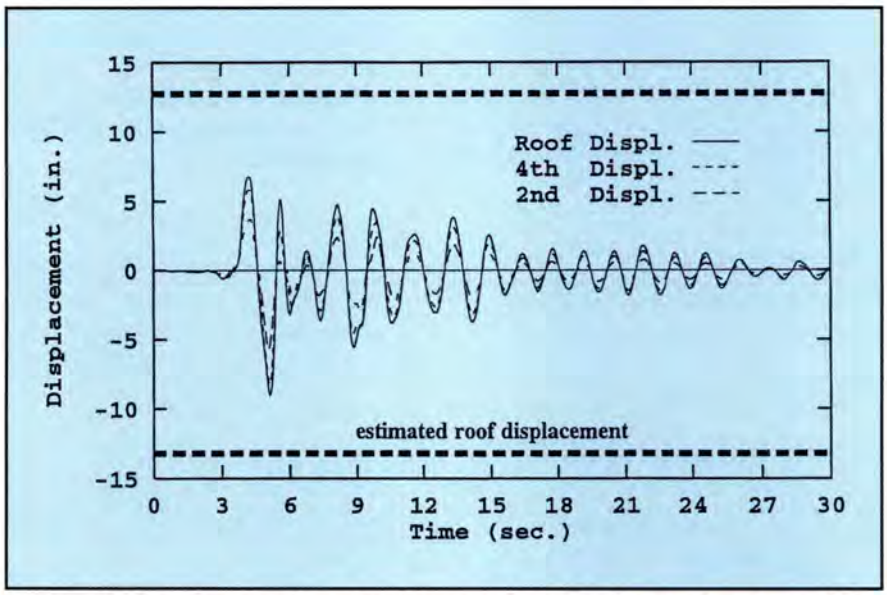

Fig. 12. Displacement time-histories of Frame 1 during NEW ground motion scaled to a peak ground acceleration of 0.4*g*. **Note:** 1 in. = 25.4 mm.

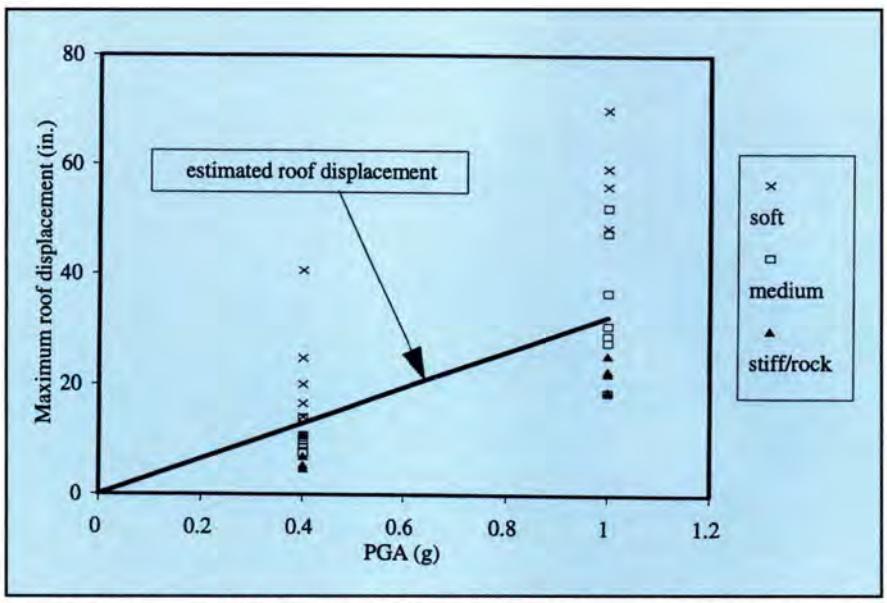

Fig. 13. Maximum roof displacement of Frame 1 vs. peak ground acceleration (PGA) of the ground motion. **Note:** 1 in. = 25.4 mm.

It should be kept in mind that the estimated roof displacements are based on elastic analysis under NEHRP[8] equivalent lateral forces for medium soil and 5 percent damping. The estimated displacements are based on the approximate period given by the 1991 edition of the NEHRP provisions[8] which is smaller than the actual period of Frame 1, as indicated in Table 4. An improved design approach would estimate the roof displacement demands using a NEHRP design spectra for the proper damping ratio, actual soil condition, and actual period of the frame.

Displacement amplification factors, similar to load factors, can be developed on a probabilistic basis to scale up the estimated roof displacements to account for the observed scatter in the displacements from dynamic analyses. These displacement amplification factors should depend on the seismic zone and the soil conditions of the building site. Suggested values of the displacement amplification factors are given in reports by El-Sheikh et al.[3,4]

Using these displacement amplification factors, Frame 1 could be redesigned to: (1) decrease the maximum roof displacement (e.g., by increasing the stiffness) during the survival level ground motions on medium and soft soil conditions to an acceptable level (e.g., 3.0 percent roof drift to prevent failure of the gravity load resisting system and maintain structural integrity); and (2) provide sufficient ductility capacities to the beam-column connections to satisfy the ductility demands.

Base Shear — Fig. 14 shows the base shear of Frame 1 during the NEW ground motion scaled to a peak ground acceleration of 1.0*g*. The dashed horizontal lines indicate the static base shear capacity of the frame obtained from push-over analysis under the inertia force distribution specified in the NEHRP[8] equivalent lateral forces procedure. The peak values of base shear reached during the dynamic analysis are significantly larger than the static base shear capacity, primarily because of the contribution of higher modes.

Effect of Inelastic Energy Dissipation and Self-Centering — The

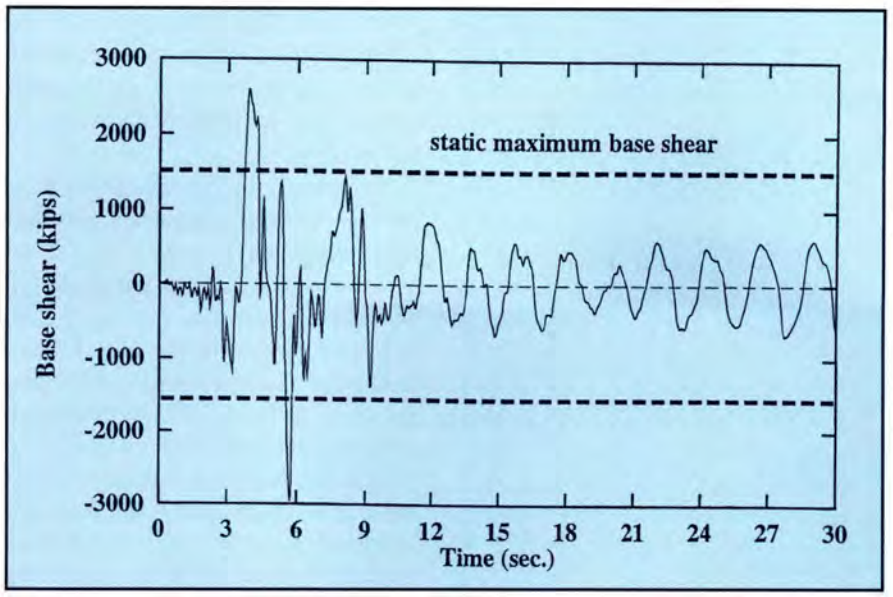

Fig. 14. Base shear time-history of Frame 1 during NEW ground motion scaled to a peak ground acceleration of 1.0*g*. **Note:** 1 kip = 4.45 kN.

effect of the inelastic energy dissipation and self-centering provided by unbonded post-tensioned precast concrete frames were investigated. The SM was used because the beam-column connection hysteresis behavior can be directly controlled by specifying different residual deformation factors (α_r).[3,4] Increases in α_r increase the energy dissipated by the beam-column connections and decrease the self-centering. Frame 1 was investigated using TRE ground motion scaled to a peak ground acceleration of 0.4*g*. Two α_r values (0.03 and 0.90) were considered.

The SM with the small α_r tends to have low energy dissipation (LED) and represents an unbonded post-tensioned precast concrete frame. The SM with the large α_r tends to have high energy dissipation (HED) and represents a conventional cast-in-place reinforced concrete frame. Fig. 15(a) shows the moment-rotation behavior of one of the first floor beam-column connections of Frame 1 modeled with the FM and the SM with low energy dissipation (LED). Fig. 15(b) shows the moment-rotation behavior of the same connection modeled with the SM with high energy dissipation (HED).

Fig. 15(a) shows a relatively good comparison between the FM and the SM with low energy dissipation, however, the increase in bending moment capacity of the beam-column connection due to the axial compression force in the first floor beams is captured only by the FM. The hysteresis

Table 6. Maximum seismic response parameters of Frame 1.

Peak ground acceleration	Soil type	Ground motion	Maximum roof displacement (in.)	Maximum roof drift (percent)	Maximum story drift (percent)	Maximum base shear (kips)
0.4*g* design level	Stiff/Rock	ELC	5.33	0.55	0.72	1378
		PRE	10.74	1.11	1.51	1795
		STF	4.74	0.49	0.87	1595
		GST	6.92	0.71	1.30	1686
	Medium	SYL	10.68	1.10	1.67	2043
		HOL	9.73	1.00	1.76	1850
		YER	13.90	1.43	1.95	1760
		ORI	10.35	1.07	1.83	1846
		NEW	9.01	0.93	1.80	2024
		MED	9.84	1.01	1.68	1757
		GME	7.53	0.78	1.30	1730
	Soft	TRE	24.74	2.55	3.46	2000
		FOS	16.55	1.70	2.47	1923
		SOF	19.98	2.06	3.31	2190
		GSO	14.11	1.45	2.19	2165
1.0*g* survival level	Stiff/Rock	ELC	22.14	2.28	2.80	2230
		PRE	18.90	1.94	3.58	2641
		STF	25.41	2.61	3.87	2757
		GST	22.60	2.33	3.41	2305
	Medium	SYL	27.71	2.85	3.75	2535
		HOL	52.26	5.38	6.42	2727
		YER	18.59	1.91	2.97	2433
		ORI	30.75	3.16	4.41	2388
		NEW	29.04	2.99	4.11	2957
		MED	36.72	3.78	5.69	2797
		GME	47.67	4.90	5.84	2716
	Soft	TRE	56.19	5.78	6.14	3000
		FOS	48.56	5.00	5.65	2716
		SOF	59.37	6.11	7.32	3122
		GSO	70.12	7.21	7.96	3063

Note: 1 in. = 25.4 mm; 1 kip = 4.45 kN.

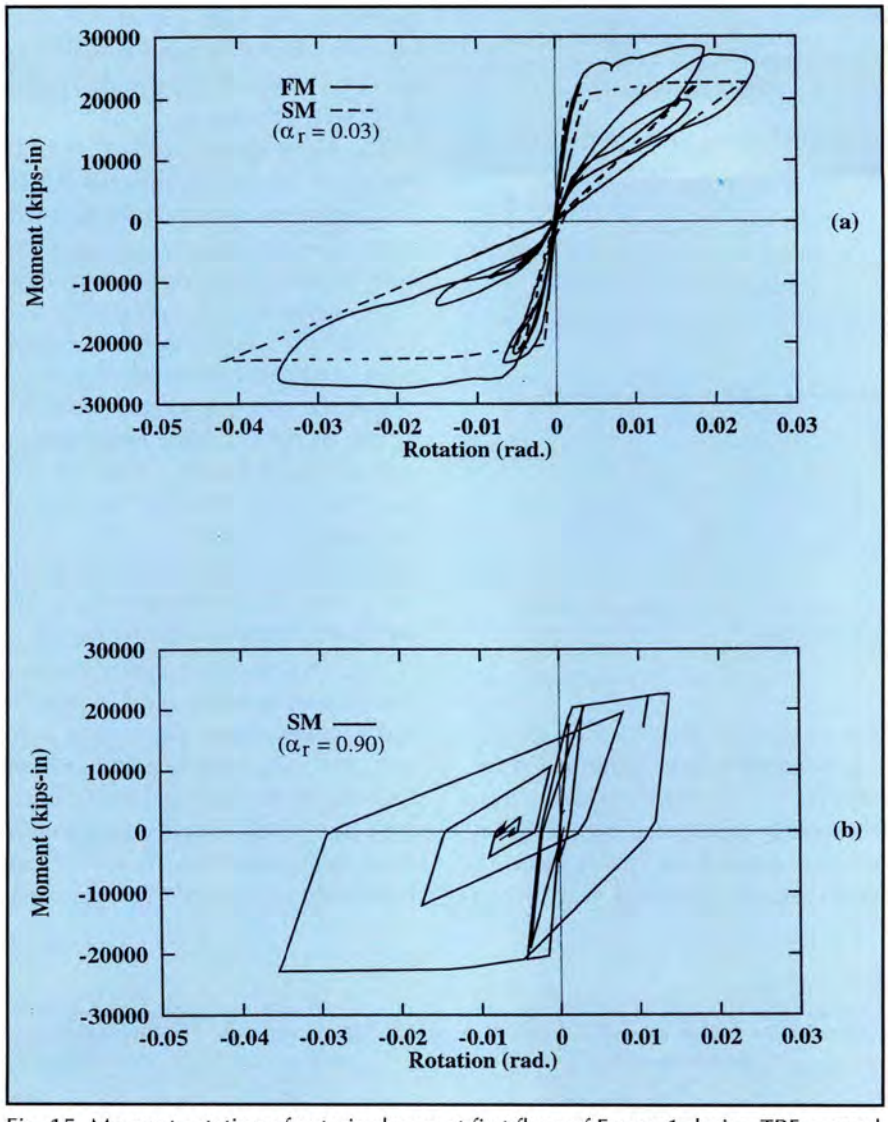

Fig. 15. Moment-rotation of exterior beam at first floor of Frame 1 during TRE ground motion scaled to a peak ground acceleration of 0.4*g*: (a) using the FM and the SM with low energy dissipation; (b) using the SM with high energy dissipation. **Note:** 1 in. = 25.4 mm; 1 kip = 4.45 kN.

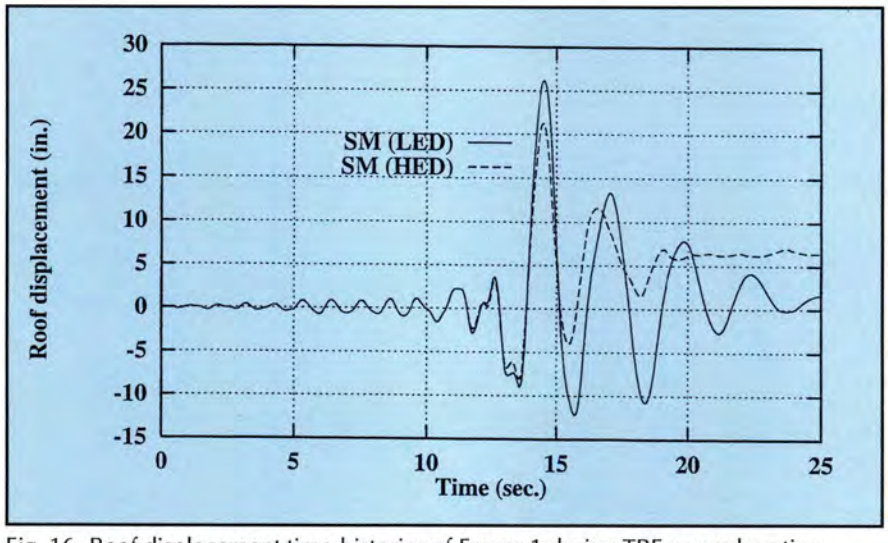

Fig. 16. Roof displacement time-histories of Frame 1 during TRE ground motion scaled to a peak ground acceleration of 0.4*g*, using the SM with low energy dissipation (LED) and high energy dissipation (HED). **Note:** 1 in. = 25.4 mm.

loops of the SM with high energy dissipation are similar to those of a stiffness-degrading model of cast-in-place reinforced concrete beam-column connections.

Comparing the hysteresis loops of the low energy dissipation and high energy dissipation cases in Fig. 15, the following observations are made: (1) the energy dissipation per loop for the high energy dissipation case is more than twice that of the low energy dissipation case; (2) the maximum rotation demand of the high energy dissipation case is less than that of the low energy dissipation case; and (3) the final hysteresis loops of the high energy dissipation case oscillate around a residual rotation, while all loops of the low energy dissipation case oscillate around zero rotation.

Fig. 16 shows roof displacement time-histories for the SM of Frame 1 with low energy dissipation and high energy dissipation during the 0.4*g* TRE ground motion. The maximum roof displacement for the high energy dissipation case is smaller than that of the low energy dissipation case by about 19 percent. The amplitude of the displacement cycles following the maximum displacement decays more rapidly for the high energy dissipation case. The low energy dissipation case has several successive large displacement cycles. On the other hand, the low energy dissipation case has self-centering (i.e., the roof displacement oscillates around zero displacement), which results in a small residual displacement.

TIME-HISTORY DYNAMIC ANALYSES OF FRAME 4

The dynamic analyses of Frame 4 show the frame performs well and satisfies the design criteria. The maximum roof displacements are significantly less than the roof displacement estimated in design. Two factors should be noted: (1) the large difference between the maximum period allowed in the NEHRP[8] design procedure (C_aT_a = 1.38 seconds) and the actual period of the frame (T = 2.48 seconds), and (2) the large contribution of the gravity load moment to the moment used to design the beam-column connections.

Table 7. Maximum seismic response parameters of Frame 4 during the TRE ground motion.

Peak ground acceleration	Maximum roof displacement (in.)	Maximum roof drift (percent)	Maximum story drift (percent)	Maximum base shear (kips)
0.1*g* design level	8.86	0.91	1.24	481
0.25*g* design level	14.6	1.51	1.97	623

Note: 1 in. = 25.4 mm; 1 kip = 4.45 kN.

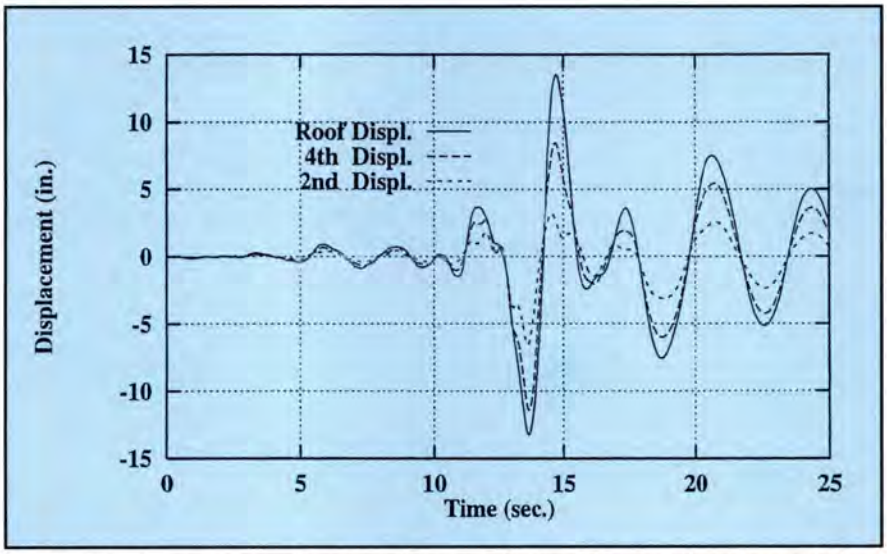

Fig. 17. Displacement time-histories of Frame 4 during TRE ground motion scaled to a peak ground acceleration of 0.25*g*. **Note:** 1 in. = 25.4 mm.

Both factors result in a significant overstrength of the base shear of the frame above the base shear used in design (V_{el}), as shown in Fig. 10. Consequently, the ductility demands are significantly less than those of Frame 1. Table 7 summarizes the dynamic response of Frame 4 during the TRE ground motion scaled to a peak ground acceleration of 0.1*g* and 0.25*g* to represent the design and the survival level ground motions, respectively. Fig. 17 shows time-histories of the lateral displacement of the roof and the second and fourth floor levels of Frame 4 during the TRE ground motion scaled to a peak ground acceleration of 0.25*g*. The maximum roof drift reaches only 1.5 percent.

CONCLUSIONS

Based on the research findings presented in this paper, the following conclusions are drawn:

1. For design, the moment-rotation behavior of a beam-column connection can be represented by a trilinear idealization developed using approximate formulas for three limit states in the behavior.

2. Unbonded post-tensioned precast frames can be designed using the design approach described in this paper. However, the design criteria should not be based on the displacements estimated using an equal displacement assumption for frames on medium or soft soil conditions in regions of high seismicity. Displacement amplification factors similar to those given in reports by El-Sheikh et al.[3,4] should be used under these conditions.

3. Local ductility demand factors (γ-factors) are needed to amplify the local ductility demands for the beam-column connections. The local ductility demand factors are larger for frames designed for high seismicity regions than for frames designed for moderate seismicity regions.

4. Compared to similar cast-in-place reinforced concrete frames, the maximum displacement of unbonded post-tensioned precast frames under seismic loading is expected to be larger, due to the small energy dissipation, while the accumulated residual displacement is expected to be much smaller.

ACKNOWLEDGMENTS

This investigation was funded by the National Science Foundation (NSF) under Grant No. BCS-9307880 as part of the Precast Seismic Structural Systems (PRESSS) research program. The support of the NSF Program Director, Dr. S. C. Liu and Program Coordinator Dr. M. J. N. Priestley is gratefully acknowledged. Financial support for the first author was provided by Cairo University, Egypt.

The investigation was carried out at the center for Advanced Technology for Large Structural Systems (ATLSS) at Lehigh University. The authors wish to thank the reviewers for their thoughtful comments. The opinions, findings, and conclusions expressed in this paper are those of the authors.

REFERENCES

1. Priestley, M. J. N., "Overview of PRESSS Research Program," PCI JOURNAL, V. 36, No. 4, July-August 1991, pp. 50-57.
2. Nakaki, S., and Englekirk, R., "PRESSS Industry Seismic Workshops: Concept Development," PCI JOURNAL, V. 36, No. 5, September-October 1991, pp. 54-61.
3. El-Sheikh, M., Pessiki, S., Sause, R., Lu, L.-W., and Kurama, Y., "Seismic Analysis, Behavior, and Design of Unbonded Post-Tensioned Precast Concrete Frames," Earthquake Engineering Research Report, Report No. EQ-97-02, Department of Civil and Environmental Engineering, Lehigh University, Bethlehem, PA, November 1997.
4. El-Sheikh, M., "Seismic Analysis, Behavior, and Design of Unbonded Post-Tensioned Precast Concrete Frames," Ph.D. Dissertation, Department of Civil and Environmental Engineering, Lehigh University, Bethlehem, PA, October 1997, 456 pp.
5. Prakash, V., Powell, G., and Campbell, S., "DRAIN-2DX Base Program Description and User Guide; Version 1.10," Report No. UCB/SEMM-93/17&18, Structural Engineering Mechanics and Materials, Department of Civil Engineering, University of California, Berkeley, CA, December 1993.
6. Cheok, G., and Lew, H. S., "Model Precast Concrete Beam-to-Column Connections Subject to Cyclic Loading," PCI JOURNAL, V. 38, No. 4, July-August 1993, pp. 80-92.
7. Priestley, M. J. N., and Tao, J., "Seismic Response of Precast Prestressed Concrete Frames with Partially Debonded Tendons," PCI JOURNAL, V. 38, No. 1, January-February 1993, pp. 58-69.
8. Building Seismic Safety Council, "NEHRP Recommended Provisions for the Development of Seismic Regulations for New Buildings," BSSC, Washington, D.C., 1991, 1994, 1997.
9. ACI Committee 318, "Building Code Requirements for Structural Concrete (ACI 318-95)," American Concrete Institute, Farmington Hills, MI, 1995.

APPENDIX — NOTATION

a = compression stress block depth
a'' = compression stress block depth, measured from inside spirals, when spiral confined concrete fails
A_p = total cross-sectional area of post-tensioning steel
b = beam cross-sectional width
b'' = beam cross-sectional width, measured from inside spirals
c'' = neutral axis depth, measured from inside spirals, when spiral confined concrete fails
C_a = period modification factor defined in NEHRP
C_d = inelastic deflection amplification factor defined in NEHRP
$c_l = f_{pl}/f_{pu}$
E_c = concrete Young's modulus of elasticity
E_p = post-tensioning steel Young's modulus of elasticity
f_c' = maximum compressive strength of unconfined concrete
f_{cc}' = maximum compressive strength of confined concrete
f_{ci} = concrete initial stress
f_{pi} = post-tensioning steel initial stress
f_{pl} = post-tensioning steel stress at its limit of proportionality (post-tensioning steel yield stress)
f_{pu} = post-tensioning steel ultimate strength
h = total height of beam
h'' = confined beam height, measured from inside spirals
L_b = beam span between inflection points
L_{bc} = beam clear length between column faces
L_{cr} = failure (crushing) length of spiral confined concrete, adjacent to beam-column interface
L_{pu} = total unbonded length of post-tensioning steel for exterior beam-column connections or half the unbonded length of post-tensioning steel for interior beam-column connections
M_{dec} = beam decompression moment (at decompression limit state)
M_{des} = beam-column connection moment for design level of earthquake loading
M_{el} = beam-column connection moment demand for reduced level of earthquake loading
M_{ll} = beam linear limit moment (at linear limit state)
M_{sur} = beam-column connection moment for survival level of earthquake loading
M_{ult} = beam ultimate moment (at ultimate limit state)
M_y = beam yield moment (at yield limit state)
R = response modification factor defined in NEHRP
T = building fundamental period
T_a = approximate period defined in NEHRP
V_{des} = design base shear
V_{el} = elastic base shear corresponding to reduced level of earthquake loading
V_{ll} = base shear at effective linear limit state
V_{sur} = survival base shear
V_{ult} = base shear at ultimate limit state
V_y = base shear at yield limit state
α = equivalent stress block coefficient for confined concrete equal to ratio of stress of stress block to maximum compressive strength of concrete
α_r = residual deformation factor
β = equivalent stress block coefficient for confined concrete equal to ratio of stress block depth to neutral axis depth
$\gamma_{des\text{-}loc}$ = local ductility demand factor for design level ground motion
$\gamma_{sur\text{-}loc}$ = local ductility demand factor for survival level ground motion
Δ_{des} = roof displacement for design level of earthquake loading
Δ_{el} = roof displacement corresponding to elastic (reduced) level of earthquake loading
Δ_{ll} = roof displacement at effective linear limit state
Δ_{sur} = roof displacement for survival level of earthquake loading
Δ_{ult} = roof displacement at ultimate limit state
Δ_y = roof displacement at yield limit state
ε_{cu} = ultimate compression strain of spiral confined concrete
θ_{all} = allowable rotation which is taken as inelastic story drift of NEHRP provisions
θ_{des} = beam-column connection rotation for design level of earthquake loading
θ_{el} = beam-column connection rotation demand for reduced level of earthquake loading
θ_{ll} = beam linear limit rotation (at linear limit state)
θ_{sur} = beam-column connection rotation for survival level of earthquake loading
θ_{ult} = beam ultimate rotation (at ultimate limit state)
θ_y = beam yield rotation (at yield limit state)
ϕ = capacity reduction factor